frontiers in Materials

ORIGINAL RESEARCH
published: 28 August 2020
doi: 10.3389/fmats.2020.00177

Dielectric and Electromagnetic Attenuated Properties of WC/Wax Composite

Weiming Yang[1], Mengxiao Sun[2], Zhiqian Yang[3], Chang Xu[3], Yilu Xia[3] and Ziming Xiong[3]**

[1] Insitute of Logistics Science and Technology, Academy of System Engineering, Academy of Military Science of Chinese PLA, Beijing, China, [2] School of Mechanical Engineering, Nanjing University of Science and Technology, Nanjing, China, [3] State Key Laboratory for Disaster Prevention & Mitigation of Explosion & Impact, Army Engineering University of PLA, Nanjing, China

In this study, tungsten carbide (WC) microparticles with different sizes were synthesized by the heating-programmed temperature method. Tungsten carbide produces obvious resonance peaks at intermediate and high frequencies, which contribute to electromagnetic absorption performance. The results show that a composite consisting of 30 vol.% WC exhibits a strongest absorption point (RL_{min}) of −71.81 dB, when the thickness is only 1.89 mm.

Keywords: tungsten carbide, dielectric properties, electromagnetic absorption, composite, resonance

OPEN ACCESS

Edited by:
Biao Zhao,
Zhengzhou University of Aeronautics, China

Reviewed by:
Isabelle Huynen,
Catholic University of Louvain, Belgium
Lianwen Deng,
Central South University, China

***Correspondence:**
Mengxiao Sun
smx0212@163.com
Ziming Xiong
xzm992311@163.com

Specialty section:
This article was submitted to Polymeric and Composite Materials, a section of the journal Frontiers in Materials

Received: *14 March 2020*
Accepted: *13 May 2020*
Published: *28 August 2020*

Citation:
Yang W, Sun M, Yang Z, Xu C, Xia Y and Xiong Z (2020) Dielectric and Electromagnetic Attenuated Properties of WC/Wax Composite. Front. Mater. 7:177. doi: 10.3389/fmats.2020.00177

INTRODUCTION

In recent years, metals and their oxide, low-dimensional carbon materials are currently the most popular materials in the research of electromagnetic absorption (EA) materials. Metal and their composites mainly include the metal with dielectric property, the ferromagnetic metal, and their oxide, for example, metal microstructure (Liu et al., 2018; Qiu et al., 2020), ZnO (Wu et al., 2014; Sun et al., 2016), CuO (Ma et al., 2016), Fe_2O_3 (Xu et al., 2019), $CoFe_2O_4$ (Zhang et al., 2019), MoS_2 (Dai et al., 2019), and so on. The minimum value of reflection loss (RL) of quasi-one-dimensional nickel nanostructure prepared by a wet chemical process reached −42.08 dB at 7.4 GHz with a low filler loading (Xu et al., 2018). When the filler loading ratio of the flower-like carbonyl iron powder was 60 wt.% in paraffin wax, the RL_{min} was −35.4 dB at 8.99 GHz (Yu et al., 2015). As the typical representative of low-dimensional carbon materials, graphene (or reduced graphene oxide) (Xia et al., 2018; Dong et al., 2019) and carbon nanotubes (CNTs) (Zhu et al., 2019; Yang et al., 2020) have good dielectric property and EA performance. Reduced graphene oxide prepared by a thermal reduction method possessed an effective EA bandwidth (RL < 10 dB) of 7.60 GHz with 1 wt.% filler loading (Wu et al., 2018). The fluorinated single-walled carbon nanotubes (SWCNTs) also have EA bandwidth of 5.10 GHz. The NiCo-SWCNTs/$CoFe_2O_4$ nanocomposites with 15 wt. % NiCo-SWCNTs exhibited the best EA performance; the EA bandwidth was up to 7.1 GHz with a matching thickness of only 1.8 mm (Fang et al., 2017). In addition, in order to adapt to the changing environment, researchers from Beijing Institute of Technology have done several works on the EA materials under variable temperature conditions, including ZnO@multi-wall carbon nanotubes (MWCNTs) (Lu et al., 2014), CdS@MWCNTs (Lu et al., 2016), PEDOT:PSS/Fe_3O_4-NG/CP (Wang et al., 2019), Fe_3O_4/MWCNTs (Lu et al., 2015),

and so on. The EA performance of substances, such as short carbon fibers (Cao et al., 2010), N doped SiC (Dou et al., 2014), rGO/SiC (Han et al., 2016), and so on, at variable temperature was also investigated. However, the test temperature range for these materials is concentrated at 300 to 700 K.

Despite the excellent EA performance of the above popular materials, there are some defects in the real application environments. Ferromagnetic EA materials demagnetize at high temperature, and this phenomenon may affect the EA performance of the materials severely. The dielectric metals and their oxide have poor corrosion resistance, and carbon materials cannot achieve large-scale preparation, which limits their further development.

High-temperature ceramic (HTC) is a new type of ceramic material with high temperature resistance. Melting point and hardness of HTC are generally higher than metal materials, and its chemical stability is excellent (Ren et al., 2017). High-temperature ceramic mainly includes oxide ceramics and non-oxide ceramics. Compared with oxide ceramics, non-oxide ceramics are characterized by good thermal shock resistance and light weight (Zhang et al., 2016). Tungsten carbide (WC) is a non-oxide HTC material and widely used in the field of cemented carbide. Moreover, because of advantages of high stability, low price, and low toxicity, it is also used as catalyst in fuel cells and air batteries. Compared with the EA materials mentioned previously, HTC can withstand higher temperature and have chemical stability at the same time. Therefore, the use of HTC in the field of Electromagnetic (EM) absorption can solve the issue that most EM absorbing materials have poor EA performance in high temperatures.

In this article, WC microparticles with different sizes were synthesized by the heating-programmed temperature method. Compared with other HTC, the dielectric property of WC microparticle is fine. Tungsten carbide produces obvious resonance peaks at intermediate and high frequencies, which contribute to EA performance.

RESULTS AND DISCUSSION

The SEM images of WC are shown in **Figures 1A,B**. It can be found that the particle size of WC-1 is $<1\,\mu m$, whereas the particle size of WC-2 is $\sim 10\,\mu m$, which is larger than WC-1. **Figure 1C** shows the X-ray diffraction (XRD) pattern of the samples. The characteristic peaks of the two samples are almost the same. The strong characteristic peaks of 31.48, 35.62, and 48.26° are indexed to the WC phase of (001), (100), and (101). The weak characteristic peaks of 63.69, 65.78, 73.06, 75.52, and 77.08° correspond to the (110), (002), (111), (200), and (102) phase of WC. The Chemical composition analysis of WC microparticle is confirmed by Energy-dispersive X-ray spectroscopy (EDS), which is shown in **Figure S1** (Supplementary Material). The chemical states and surface elements of the WC microparticle were investigated by X-ray photoelectron spectroscopy (XPS) shown in **Figures 1D–F**. The peaks located around 282.7, 34.3, and 32.1 eV are assigned to the C 1 s and W 4 f of the WC, respectively. The results of

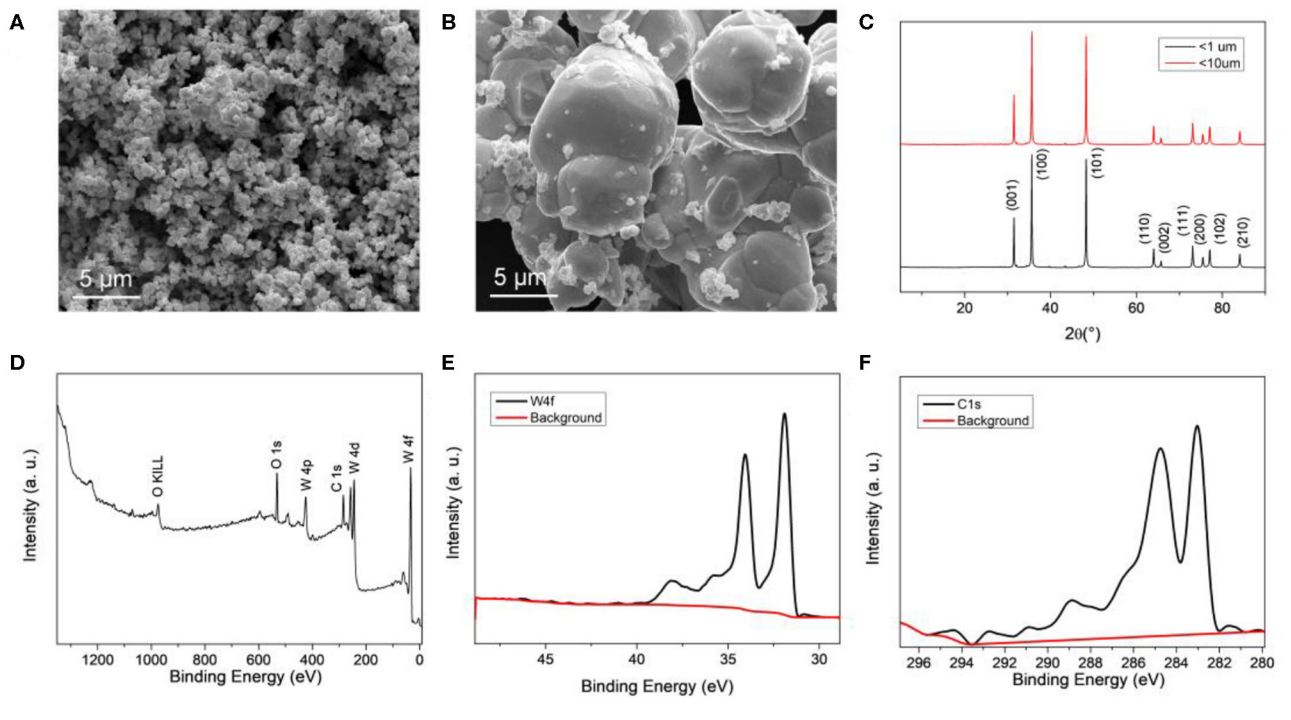

FIGURE 1 | SEM image of WC-1 **(A)** and WC-2 **(B)**; XRD pattern **(C)** and XPS spectra **(D–F)** of WC.

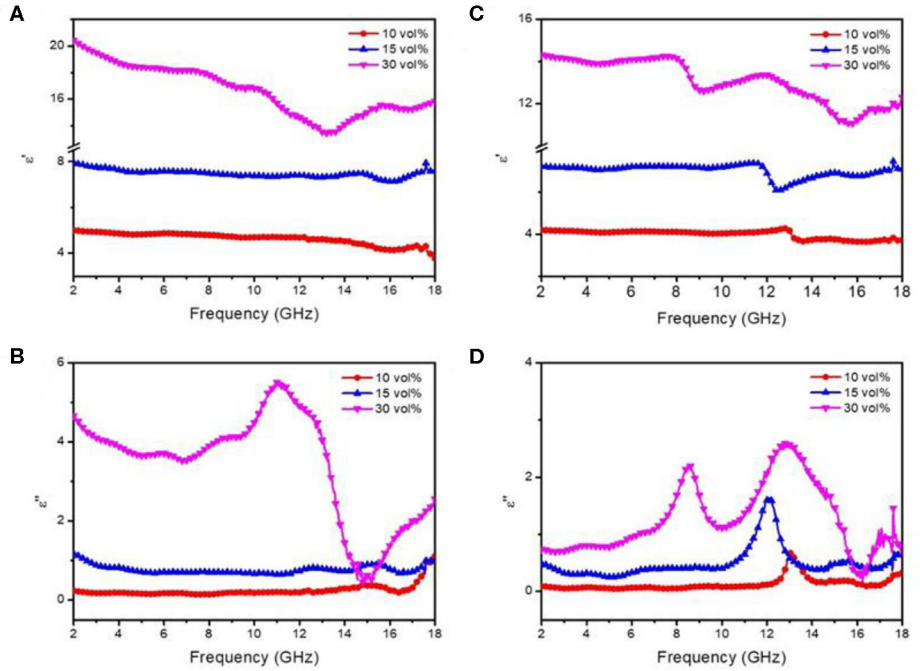

FIGURE 2 | Real part (ε') and imaginary part (ε'') of relative complex permittivity of WC-1 **(A,B)** and WC-2 **(C,D)** with different filler loadings.

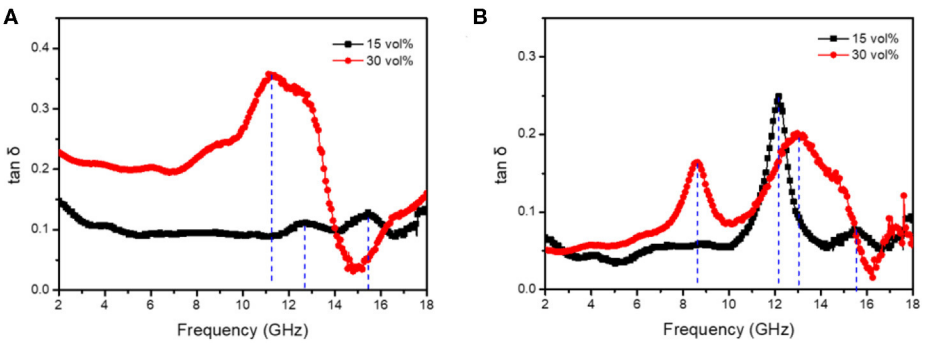

FIGURE 3 | Tangent loss of WC-1 **(A)** and WC-2 **(B)** with different filler loadings.

XPS are consistent with the conclusion obtained by XRD. The thermal stability of WC was tested by TGA, and the result is shown in **Figure S2**. The weight loss of WC is almost unchanged at the test temperature (273–1,073 K), and it shows excellent thermal stability.

The relative complex permittivity (ε' and ε'') of WC/wax is shown in **Figure 2**. It is well-known that the storage capacity and dissipation capacity of the electromagnetic energy can be described by ε' and ε'', respectively. It can be found that the values of ε' and ε'' increase with the increasing filler loading of WC, which can be interpreted by the effective medium theory. At the same filler loading, it can be obviously seen that ε' and ε'' values of WC-1 are higher than WC-2, indicating better storage capacity and dissipation capacity of the electromagnetic energy. Moreover, WC-1 and WC-2 exhibit certain fluctuations in the curves of ε' and ε'', and the resonance peaks of ε'' are more obvious than ε' at same filler loading.

In order to further analysis the dielectric loss capability of WC-1 and WC-2 with different filler loadings, **Figure 3** shows tangent loss ($\tan\delta = \varepsilon''/\varepsilon'$) of WC-1 and WC-2 with the filler loadings of 15 and 30 vol%. The $\tan\delta$ value of the samples shows an upward trend in the most part of 2 to 18 GHz with the increasing filler loading. Generally, higher $\tan\delta$ means better dielectric loss. When the filler loading is 15 vol%, the $\tan\delta$ resonance peaks of WC-1 are near 11.2 and 15.4 GHz, and the $\tan\delta$ resonance peaks of WC-2 are near 12.1 and 15.6 GHz. When the filler loading is 30 vol%, the $\tan\delta$ resonance peaks of WC-1 are near 11.2 and 18 GHz, and the $\tan\delta$ resonance peaks of WC-2 are near 8.6 and 13.1 GHz.

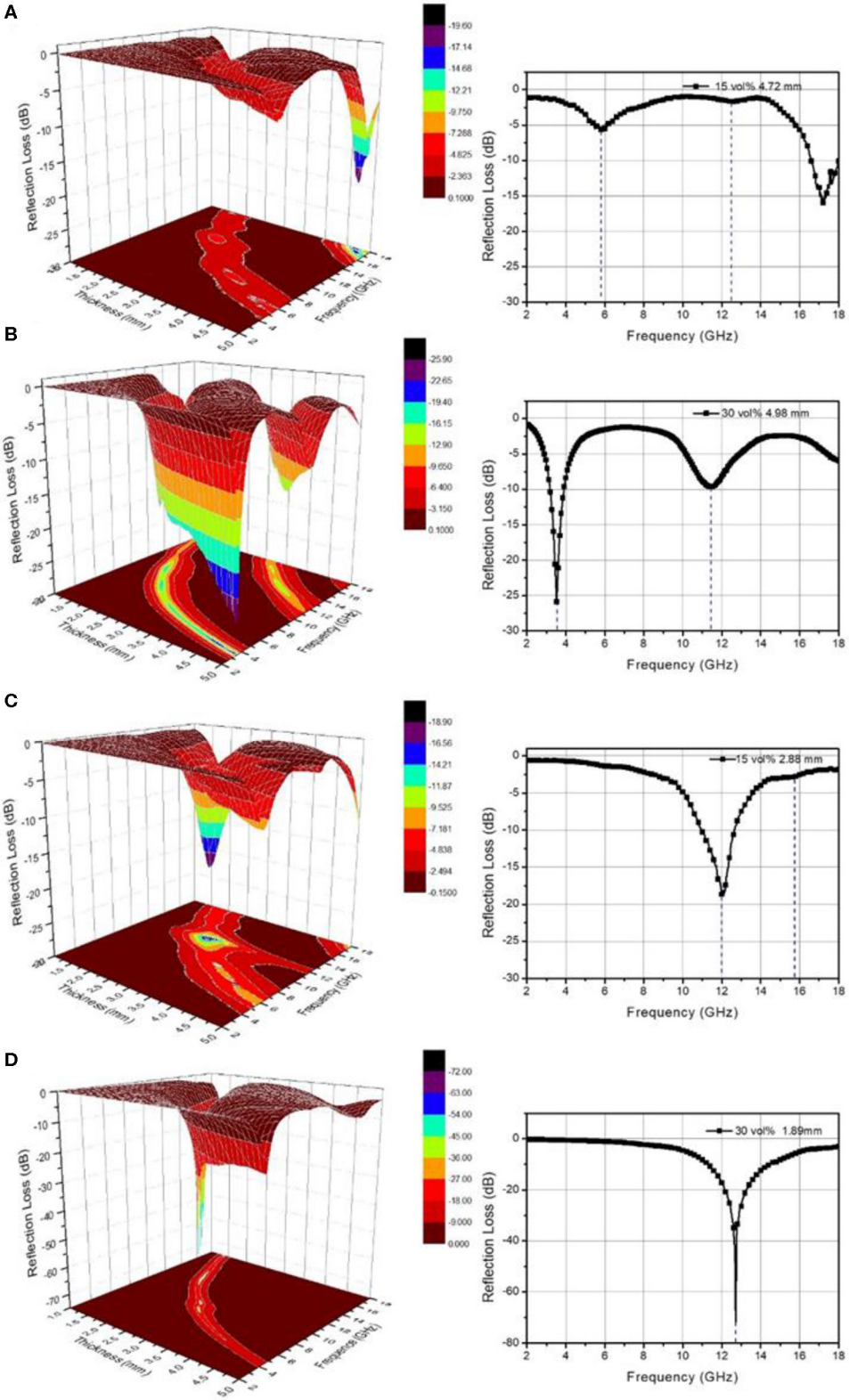

FIGURE 4 | Frequency dependence of 3D plots and the optimal reflection loss (RL_{min}) curve of WC-1 **(A,B)** and WC-2 **(C,D)**.

TABLE 1 | EA performance of WC-1 and WC-2.

Sample	Filler loading (vol. % in wax)	Thickness (mm)	RL_{min} (dB)	Corresponding frequency (GHz)
WC-1	15	4.72	−19.51	17.64
WC-1	30	4.98	−25.87	3.52
WC-2	15	2.66	−18.88	12.40
WC-2	30	1.89	−71.81	12.72

According to the free electron theory and Debye theory, ε' and ε'' can be expressed as follows:

$$\varepsilon' = \varepsilon_\infty + \frac{\varepsilon_s - \varepsilon_\infty}{1 + (2\pi f)^2 \tau^2}$$

$$\varepsilon'' = \varepsilon_p{}'' + \varepsilon_c{}'' = (\varepsilon_s - \varepsilon_\infty) \frac{2\pi f \tau}{1 + (2\pi f)^2 \tau^2} + \frac{\sigma}{2\pi f \varepsilon_0}$$

where ε_s is the stationary dielectric constant, ε_∞ is the optical dielectric constant, f the frequency, τ is the polarization relaxation time, σ is the conductivity, $\varepsilon_p^{''}$ is the polarization loss part, and $\varepsilon_c^{''}$ is the conductive loss part. When the effect of conduction loss is not considered, the relation between $\varepsilon^{'}$ and $\varepsilon^{''}$ can be written as

$$\left(\varepsilon' - \frac{\varepsilon_s + \varepsilon_\infty}{2}\right)^2 + \left(\varepsilon''\right)^2 = \left(\frac{\varepsilon_s - \varepsilon_\infty}{2}\right)^2$$

Generally, a hemicycle curve of ε' and ε'', which is named as Cole-Cole semicircle, represents a Debye relaxation process. As shown in **Figure S3**, both of the two samples have obviously Cole-Cole semicircles, which prove Debye relaxation behaviors. And the Cole-Cole semicircle of WC-2 is the most obvious at the filler loading of 15 vol%, which means the Debye relaxation behavior of WC-2 at 15 vol% is superior to other samples. In addition, the irregular semicircles also indicate that extra loss mechanisms also exist, such as Maxwell–Wagner relaxation, electron polarization, and conductive loss.

The microwave absorption performance is generally evaluated by RL, which can be calculated as the following equations:

$$Z_{in} = Z_0 \sqrt{\frac{\mu_r}{\varepsilon_r}} tanh\left(j\frac{2\pi f d}{c}\sqrt{\varepsilon_r \mu_r}\right)$$

$$RL\left(\mathrm{dB}\right) = 20\lg\left|\frac{Z_{in} - Z_0}{Z_{in} + Z_0}\right|$$

where μ_r and ε_r are the relative complex permeability and permittivity, respectively; c is the velocity of EM waves in free space; f is the frequency; and d is the thickness. **Figure 4** shows the 3D RL and the optimal RL curve of WC with the filler loading of 15 and 30 vol%, respectively. As shown in **Table 1**, it can be found that WC-2 shows the best microwave absorption performance; when filler loading is 30 vol%, the optimal RL can reach −71.81 dB at frequency of 12.72 GHz, which corresponds to the resonance peak of tanδ shown in **Figure 3B**. Furthermore, it can be also found that both of the two samples show better microwave absorption with the increasing filler loading. And the microwave absorption performance of WC-2 is better than WC-1 at the same filler loading.

CONCLUSIONS

In summary, WC with different scales was synthesized by a heating-programmed temperature method, and the dielectric of WC investigated and its application prospects as EA materials was discussed for the first time. Compared with other HTCs, the dielectric property of WC microparticle is fine. Tungsten carbide produces obvious resonance peaks at intermediate and high frequencies, which contribute to EA performance. The real part and imaginary part of relative complex permittivity of WC-1 were higher than WC-2 with the same filler loading ratio at 2- to 18-GHz test frequency. In terms of EA performance, WC-2 was better than WC-1. This result shows that high dielectric constant does not mean that it has excellent EA performance.

DATA AVAILABILITY STATEMENT

All datasets generated for this study are included in the article/**Supplementary Material**.

AUTHOR CONTRIBUTIONS

MS and ZX conceived the idea for the research. WY, ZY, CX, and YX carried out the experiments. All authors collaborated on finalizing the manuscript.

SUPPLEMENTARY MATERIAL

The Supplementary Material for this article can be found online at: https://www.frontiersin.org/articles/10.3389/fmats.2020.00177/full#supplementary-material

REFERENCES

Cao, M., Song, W., Hou, Z., Wen, B., and Yuan, J. (2010). The effects of temperature and frequency on the dielectric properties, electromagnetic interference shielding and microwave-absorption of short carbon fiber/silica composites. *Carbon* 48, 788–796. doi: 10.1016/j.carbon.2009.10.028

Dai, J., Yang, H., Wen, B., Zhou, H., Wang, L., and Lin, Y. (2019). Flower-like MoS_2@$Bi_2Fe_4O_9$ microspheres with hierarchical structure as electromagnetic wave absorber. *Appl. Surf. Sci.* 479, 1226–1235. doi: 10.1016/j.apsusc.2019.02.049

Dong, J., Lin, Y., Zong, H., Yang, H., Wang, L., and Dai, Z. (2019). Three-dimensional architecture reduced graphene oxide–$LiFePO_4$ composite:

preparation and excellent microwave absorption performance. *Inorg. Chem.* 58, 2031–2041. doi: 10.1021/acs.inorgchem.8b03043

Dou, Y., Li, J., Fang, X., Jin, H., and Cao, M. (2014). The enhanced polarization relaxation and excellent high-temperature dielectric properties of N-doped SiC. *Appl. Phys. Lett.* 104:052102. doi: 10.1063/1.4864062

Fang, Y., Tang, X., Sun, X., Zhang, Y., Zhao, J., Yu, L., et al. (2017). Preparation and enhanced microwave absorption properties of Ni-Co attached single-walled carbon nanotubes and $CoFe_2O_4$ nanocomposites. *J. Appl. Phys.* 121:224301. doi: 10.1063/1.4984937

Han, M., Yin, X., Duan, W., Ren, S., Zhang, L., and Cheng, L. (2016). Hierarchical graphene/SiC nanowire networks in polymer-derived ceramics with enhanced electromagnetic wave absorbing capability. *J. Eur. Ceram. Soc.* 36, 2695–2703. doi: 10.1016/j.jeurceramsoc.2016.04.003

Liu, Y., Zhang, Y., Zhang, C., Huang, B., Wang, X., Li, Y., et al. (2018). Aligned fluorinated single-walled carbon nanotubes as a transmission channel towards attenuation of broadband electromagnetic waves. *J. Mater. Chem. C* 6, 9399–9409. doi: 10.1039/C8TC02522C

Lu, M., Cao, M., Chen, Y., Cao, W., Liu, J., Shi, H., et al. (2016). Multiscale assembly of grape-like ferroferric oxide and carbon nanotubes: a smart absorber prototype varying temperature to tune intensities. *ACS Appl. Mater. Interfaces* 7, 19408–19415. doi: 10.1021/acsami.5b05595

Lu, M., Cao, W., Shi, H., Fang, X., Yang, J., Hou, Z., et al. (2014). Multi-wall carbon nanotubes decorated with ZnO nanocrystals: mild solution-process synthesis and highly efficient microwave absorption properties at elevated temperature. *J. Mater. Chem. A* 2, 10540–10547. doi: 10.1039/C4TA01715C

Lu, M., Wang, X., Cao, W., Yuan, J., and Cao, M. (2015). Carbon nanotube-CdS core–shell nanowires with tunable and high-efficiency microwave absorption at elevated temperature. *Nanotechnology* 27:065702. doi: 10.1088/0957-4484/27/6/065702

Ma, J., Zhang, X., Liu, W., and Ji, G. (2016). Direct synthesis of MOF-derived nanoporous CuO/carbon composites for high impedance matching and advanced microwave absorption. *J. Mater. Chem. C* 4, 11419–11426. doi: 10.1039/C6TC04048A

Qiu, Y., Lin, Y., Yang, H., Wang, L., Wang, M., and Wen, B. (2020). Hollow Ni/C microspheres derived from Ni-metal organic framework for electromagnetic wave absorption. *Chem. Eng. J.* 383, 123207. doi: 10.1016/j.cej.2019.123207

Ren, P., Zhang, K., Du, S., Zhao, Z., Wen, M., and Zheng, W. (2017). Achieving highly hydrophobic or hydrophilic HfN_x-Ag films surfaces by controlling the existing forms of Ag. *Mater. Lett.* 207, 161–164. doi: 10.1016/j.matlet.2017.07.068

Sun, M., Lv, X., Xie, A., Jiang, W., and Wu, F. (2016). Growing 3D ZnO nano-crystals on 1D SiC nanowires: enhancement of dielectric properties and excellent electromagnetic absorption performance. *J. Mater. Chem. C* 4, 8897–8902. doi: 10.1039/c6tc03162e

Wang, X., Shu, J., Cao, W., Zhang, M., Yuan, J., and Cao, M. (2019). Eco-mimetic nanoarchitecture for green EMI shielding. *Chem. Eng. J.* 369, 1068–1077. doi: 10.1016/j.cej.2019.03.164

Wu, F., Xia, Y., Wang, Y., and Wang, M. (2014). Two-step reduction of self-assembled three-dimensional (3D) reduced graphene oxide (RGO)/zinc oxide (ZnO) nanocomposites for electromagnetic absorption. *J. Mater. Chem. A* 2, 20307–20315. doi: 10.1039/c4ta04959d

Wu, F., Zeng, Q., Xia, Y., Sun, M., and Xie, A. (2018). The effects of annealing temperature on the permittivity and electromagnetic attenuation performance of reduced graphene oxide. *Appl. Phys. Lett.* 112, 192902. doi: 10.1063/1.5028472

Xia, Y., Wang, J., Chen, C., Huo, D., Wen, Y., Wang, W., et al. (2018). Controlled hydrothermal temperature provides tunable permittivity and an improved electromagnetic absorption performance of reduced graphene oxide. *RSC Adv.* 8, 33065–33071. doi: 10.1039/c8ra05843a

Xu, C., Sun, M., Yang, Z., Sun, Y., Wu, F., and Xie, A. (2019). Magnetized polypyrrole and its enhanced electromagnetic attenuation performance. *Appl. Phys. Lett.* 115:013101. doi: 10.1063/1.5100545

Xu, W., Pan, Y., Wang, G., and Qu, P. (2018). Microwave absorption enhancement and dual-nonlinear magnetic resonance of ultra small nickel with quasi-one-dimensional nanostructure. *Appl. Surf. Sci.* 428, 54–60. doi: 10.1016/j.apsusc.2017.09.052

Yang, H., Wen, B., and Wang, L. (2020). Carbon nanotubes modified CoZn/C composites with rambutan-like applied to electromagnetic wave absorption. *Appl. Surf. Sci.* 509:145336. doi: 10.1016/j.apsusc.2020.145336

Yu, M., Yang, P., Fu, J., and Liu, S. (2015). Flower-like carbonyl iron powder modified by nanoflakes: Preparation and microwave absorption properties. *Appl. Phys. Lett.* 106:161904. doi: 10.1063/1.4919064

Zhang, K., Li, J., Wu, F., Sun, M., Xia, Y., and Xie, A. (2019). Sandwich $CoFe_2O_4$/RGO/$CoFe_2O_4$ nanostructures for high-performance electromagnetic absorption. *ACS Appl. Nano Mater.* 2, 315–324. doi: 10.1021/acsanm.8b01927

Zhang, Q., Tong, H., Jian, C., Lu, Y., Yang, T., Yao, X., et al. (2016). High recoverable energy density over a wide temperature range in Sr modified (Pb,La)(Zr,Sn,Ti)O3 antiferroelectric ceramics with an orthorhombic phase. *Appl. Phys. Lett.* 109:262901. doi: 10.1063/1.4973425

Zhu, S., Xing, C., Wu, F., Zuo, X., Zhang, Y., Yu, C., et al. (2019). Cake-like flexible carbon nanotubes/graphene composite prepared via a facile method for high-performance electromagnetic interference shielding. *Carbon* 145, 259–265. doi: 10.1016/j.carbon.2019.01.030

Conflict of Interest: The authors declare that the research was conducted in the absence of any commercial or financial relationships that could be construed as a potential conflict of interest.